

THE DETONATION MECHANISM OF THE PULSATIONALLY-ASSISTED GRAVITATIONALLY-CONFINED DETONATION MODEL OF TYPE IA SUPERNOVAE

G. C. JORDAN IV,^{1,2} C. GRAZIANI,^{1,2} R. T. FISHER,³ D. M. TOWNSLEY,⁴ C. MEAKIN,^{5,6} K. WEIDE,^{1,2} L. B. REID,^{7,8}
J. NORRIS,¹ R. HUDSON,¹ D. Q. LAMB,^{1,2,9}

Draft version September 5, 2018

ABSTRACT

We describe the detonation mechanism comprising the “Pulsationally Assisted” Gravitationally Confined Detonation (GCD) model of Type Ia supernovae (SNe Ia). This model is analogous to the previous GCD model reported in Jordan et al. (2008); however, the chosen initial conditions produce a substantively different detonation mechanism, resulting from a larger energy release during the deflagration phase. The resulting final kinetic energy and ⁵⁶Ni yields conform better to observational values than is the case for the “classical” GCD models. In the present class of models, the ignition of a deflagration phase leads to a rising, burning plume of ash. The ash breaks out of the surface of the white dwarf, flows laterally around the star, and converges on the collision region at the antipodal point from where it broke out. The amount of energy released during the deflagration phase is enough to cause the star to rapidly expand, so that when the ash reaches the antipodal point, the surface density is too low to initiate a detonation. Instead, as the ash flows into the collision region (while mixing with surface fuel), the star reaches its maximally expanded state and then contracts. The stellar contraction acts to increase the density of the star, including the density in the collision region. This both raises the temperature and density of the fuel-ash mixture in the collision region and ultimately leads to thermodynamic conditions that are necessary for the Zel’dovich gradient mechanism to produce a detonation. We demonstrate feasibility of this scenario with three 3-dimensional (3D), full star simulations of this model using the FLASH code. We characterized the simulations by the energy released during the deflagration phase, which ranged from 38% to 78% of the white dwarf’s binding energy. We show that the necessary conditions for detonation are achieved in all three of the models.

Subject headings: hydrodynamics — nuclear reactions, nucleosynthesis, abundances — supernovae:general — white dwarfs

1. INTRODUCTION

Type Ia supernovae (SNe Ia) are among the most energetic explosions in the known universe, releasing $\sim 10^{51}$ ergs of kinetic energy in their ejecta, and synthesizing $\sim 0.7 M_{\odot}$ of radioactive ⁵⁶Ni. The discovery of the Phillips relation (Phillips 1993) has enabled the use of SNe Ia as standardizable cosmological candles which greatly enhances the accurate determination of their distance. The discovery of the accelerated expansion of the universe using SNe Ia (Riess et al. 1998; Perlmutter et al. 1999) has stimulated a tremendous amount of interest in the use of SNe Ia events as standard cosmological candles, allowing them to serve as probes of the equation of state

of dark energy, as parameterized by the EOS parameter $w = P/\rho$. The main challenge to the enterprise of measuring $w(z)$ using SNe Ia is reducing the systematic errors in the accuracy with which such supernovae can be used as standard candles (Dark Energy Task Force 2006). The accuracy must be improved from the current level of about 15% to about 1% in order for large surveys to determine the values of $w(z = 0)$ and its rate of change with z to better than 10% (Kim et al. 2004). The best hope for improvements in distance modulus accuracy is more accurate modeling of SNe Ia explosions.

Evidence suggests that SNe Ia are the results of the thermonuclear explosion of a carbon-oxygen (C-O) white dwarf (WD). The leading scenario for SNe Ia explosions is the single-degenerate model in which a progenitor WD accretes material from a non-degenerate companion star until the mass of the WD grows nearly equal to the Chandrasekhar limit (Whelan & Iben 1973; Nomoto 1982). The WD then manages to release enough nuclear energy by fusing C and O into radioactive Ni and other lighter α -elements in the time span of a few seconds or less (Nomoto et al. 1984), such that it deposits approximately 10^{51} ergs of energy, unbinding the star and accelerating the stellar material to speeds of thousands of kilometers per second (Branch et al. 1982).

This rapid fusion process must proceed in two phases (Niemeyer & Woosley 1997; Röpke et al. 2007a). The first phase begins with the initiation of a subsonic nuclear burning front (referred to as a deflagration or flame). As

¹ Flash Center For Computational Science, The University of Chicago, Chicago, IL 60637.

² Department of Astronomy and Astrophysics, The University of Chicago, Chicago, IL 60637.

³ University of Massachusetts Dartmouth, Department of Physics, 285 Old Westport Road, North Dartmouth, 02740.

⁴ Department of Physics and Astronomy, The University of Alabama, Tuscaloosa, AL 35487.

⁵ Steward Observatory, University of Arizona, Tucson, AZ 85721.

⁶ Theoretical Division, Los Alamos National Laboratory, Los Alamos, NM 87545.

⁷ Western Australian Geothermal Centre of Excellence, CSIRO CESRE, Kensington, WA 6151 Australia

⁸ School of Environmental Systems Engineering, University of Western Australia, Crawley WA 6009 Australia

⁹ Enrico Fermi Institute, The University of Chicago, Chicago, IL 60637.

the WD accretes material from its companion, convective carbon burn begins in its core. When carbon burning becomes too vigorous for convective cooling to be effective, a thermonuclear flame (or deflagration) is born in local hot spots that form in the convective region. The deflagration burns and rises due to buoyancy as it makes its way from the core to the outer layers of the star.

The second phase consists of a supersonic burning front — a detonation — that consumes the remainder of the WD. The transition from the deflagration phase to the detonation phase is poorly understood, and has been the subject of much modeling research. A variety of models incorporates the scenario of a deflagration followed by a detonation, such as the deflagration-to-detonation transition (DDT) (Khokhlov 1991; Gamezo et al. 2004, 2005), the pulsating reverse detonation (PRD) (Bravo & García-Senz 2009; Bravo et al. 2009), or the gravitationally confined detonation GCD (Townsend et al. 2007; Jordan et al. 2008, 2009; Meakin et al. 2009). These models differ primarily in the method by which the deflagration leads to a detonation.

An alternative scenario to the single-degenerate model is the double-degenerate model in which two WDs forming a binary system undergo a merger process that leads to the detonation of one of the WDs. The double-degenerate channel (Webbink 1984; Iben & Tutukov 1984) has recently received revived attention from both observation (e.g., Maoz et al. (2010)) and theory (e.g., van Kerkwijk et al. (2010); Zhu et al. (2011)). However, while computational models have explored prompt detonations in near-equal mass super-Chandrasekhar mergers (Pakmor et al. 2010, 2011) and head-on collisions of binary WD systems (Raskin et al. 2009; Rosswog et al. 2009) it remains unclear whether more commonplace mergers between two typical C-O WDs of masses $\sim 0.6M_{\odot}$ will result in a Type Ia explosion. Previous one-dimensional theoretical models suggest that such mergers will result in deflagration wave that sets off an accretion-induced collapse to a neutron star (Nomoto & Kondo 1991; Saio & Nomoto 1998, 2004; Shen et al. 2011).

In this work we focus on the GCD scenario of the single-degenerate model of SNe Ia. We use the FLASH code (Fryxell et al. 2000; Dubey et al. 2009) to extend the set of 3D whole-star GCD models in Jordan et al. (2008) (hereafter J08) to include multiple ignition points as initial conditions. These initial conditions provide more burning, and hence more energy release during the deflagration phase. The purpose of this work is to examine the conditions produced in the WD resulting from a scenario where more energy is released during the deflagration phase than in the previous GCD models and to demonstrate that the scenario manifests the necessary conditions for a detonation.

To distinguish between the two versions of GCD models we refer to the previous body of GCD models (Townsend et al. (2007), J08, Meakin et al. (2009), and references therein) as “classical” GCD models and refer to models in this paper as “pulsationally-assisted” GCD models or simply “pulsational” GCD (PGCD) models. The origin of the name stems from the fact that the WDs in the models undergo a pulsation where they first expand due to energy input from the deflagration phase and then contract from the pull of gravity. These models

require the contraction of the WD to create the thermodynamic conditions necessary to initiate a detonation, hence the phrase “pulsationally-assisted”. In fact, the paradigm we put forth has characteristics of both the classical GCD models and the PRD models.

In section 2 we review the classical GCD model, introduce the PGCD model, and discuss the ignition of the deflagration. In section 3 we discuss the Zel’dovich gradient mechanism as a detonation trigger and its implications for the PGCD. We additionally discuss the numerical detonation trigger used in our simulations. We give an overview of the FLASH code and the relevant physics modules used for our SNe Ia simulations in section 4. In section 5 we describe the results of our simulations. We compare the detonation mechanisms between the classical GCD and the PGCD models in section 6. Finally, in section 7 we discuss properties of the simulations as well as possible observational features of the models.

2. DISCUSSION OF GCD MODELS

2.1. *Classical GCD*

The classical GCD model of SNe Ia falls under the general category of single-degenerate models. In the GCD scenario, an off-centered deflagration ignites and begins burning its way through the star. The deflagration burns and rises, forming a plume of ash whose volume is bounded by the flame. When the plume reaches the stellar surface, the ash breaks through and spreads around the star. The ash then collides with itself at a location on the star opposite that of breakout. During this collision process, cold, low-density fuel is pushed ahead of the ash flows. The ash flows compress and heat the fuel in the collision region. By squeezing the fuel in the collision region, a jet is formed. The jet pushes the hot, smoldering fuel towards the high density layers of the WD which leads to conditions necessary to trigger a detonation (J08, Meakin et al. (2009)). The detonation occurs between 1.5 s and 3 s after ignition, which is about the time it takes for the ash to flow around the stellar surface.

In the classical GCD scenario, the deflagration does not drive the WD to expand energetically due to the fact that the deflagration is so weak. Typically, deflagration phase only release $\sim 10\%$ of the binding energy to the WD. The star has only mildly expanded by the time the ash flows have triggered a detonation, and in fact the star is still expanding when the detonation is triggered. Additionally, as reported in J08 classical GCDs produce more than $1 M_{\odot}$ of ^{56}Ni which correspond to over-luminous SNe Ia.

2.2. *Pulsationally-Assisted GCD*

In this work we introduce the PGCD scenario. The PGCD proceeds similarly to the classical GCD. An off-centered deflagration ignites and burns its way to the surface. The ash breaks through the surface of the star, some of which flows laterally over the surface towards the collision region. The PGCD differs from the classical GCD in the amount of energy released during the deflagration phase. In the classical GCD scenario, a relatively small amount of energy is released during the deflagration phase; instead, substantially more is released during the deflagration phase in the PGCD scenario. The WD

in the PGCD scenario responds to the deflagration by expanding rapidly. By the time the ash flows reach the collision region, the density has significantly dropped and the flows can not compress the fuel to the high temperatures and densities as in the classical GCD. Thus, a detonation does not immediately occur as it did in the classical GCD. However, as the ash flowed towards the collision region, it mixed with fuel on the WD surface, forming a mixing layer at the interface between the ash and surface fuel. After the collision, the mixture pushes its way into the surface layers of the star. Meanwhile, the WD has reached maximum expansion and begins to contract. As the WD contracts, it squeezes the fuel-ash mixture to high temperatures and densities. The conditions obtained are above the threshold necessary to trigger a detonation. Thus, it is the stellar contraction, and not just the kinetic energy in the ash flows themselves (as in the classical GCD), that gives rise to conditions that make it possible for the mixture to detonate.

2.3. Ignition of the Deflagration

The simulations of the classical GCD model in J08 were initiated with a single ignition point that was offset from the center of the WD. These initial conditions lead to a weak deflagration which gives rise to the events described in section 2.1. We extended our set of initial classical GCD models by choosing initial conditions that would lead to more burning — and thus releases more energy — than we had previously obtained. To accomplish this we chose to initialize our simulations with a single cluster of multiple ignition points that was offset from the center of the WD. These initial conditions serve to represent two physical situations that may occur in the WD. First, it may be possible that ignition occurs at multiple points. Recent work by Zingale et al. (2011) and Nonaka et al. (2012) of the last moments of the smoldering phase before ignition conclude that a single ignition point is the most probable scenario; however, ignition is an inherently stochastic process and many realizations are required to make definitive statements about all of the possible outcomes. Currently only a handful of simulations exist. Furthermore, the process of forming hot spots in the simulations that eventually lead to an ignition may be resolution dependent as stated in Nonaka et al. (2012), and leaves open the door for a multiple ignition point scenario. Finally, all but one of the simulations in Zingale et al. (2011) and Nonaka et al. (2012) were stopped once a hot spot formed that lead to ignition. Therefore, it may have been possible for more ignition points to form after the initial runaway, even though in the specific simulation that they continued past the formation of initial ignition point no secondary ignition points were observed. Second, though we ignore the convective turbulence, most likely convective plumes exist with a velocity ~ 100 km/s (Nonaka et al. 2012). This is comparable to the flame speed and can potentially grow the flame surface through the Kelvin-Helmholtz instability. We essentially mock-up this effect by initializing our simulations with multiple ignition points in close proximity to one another. These ignition points in turn quickly merge and form a single asymmetric burning region enclosed by a distorted flame surface.

3. DETONATION MECHANISM

3.1. Theory

3.1.1. Discussion of the Zel'dovich Gradient Mechanism

In the PGCD model, a plume of ash, with a layer mixed with fuel, plunges into the star during its contraction phase and initiates a detonation. Initially, as the plume advances around the star, a mixing layer of cold fuel and hot ash forms at the star-ash interface. Compression due to the stellar contraction and to the flow pushing to higher density layers of the star acts to heat the mixture. The composition in the mixing layer transitions from pure, hot ash in the plume to pure, cold fuel in the star, resulting in a compositional and temperature gradient in the mixing layer. A spontaneous detonation is triggered by the Zel'dovich gradient mechanism (Zel'dovich et al. 1970) when the mixture reaches the critical conditions.

The Zel'dovich mechanism requires an induction time gradient resulting from a gradient in temperature or gradients in temperature and composition. Rapid combustion in the high temperature region results in a shock wave as the burning front progresses to regions of low temperature. A detonation is formed if the gradients are shallow enough and the combustion becomes associated with the shock; otherwise, the shock wave runs ahead of the burning front and the plasma does not detonate.

For the purposes of this work, we wish to characterize the conditions under which a detonation would occur in the mixing layer that is formed when the ash plume flowed from its breakout point until it reaches the collision region. In the envisaged scenario, the mixing layer consists of a compositional gradient between pure ash in the plume and pure fuel on the surface of the WD, as well as a temperature gradient produced by combining the varying amounts of hot fuel and cold ash. In the following we discuss the critical conditions that are necessary to trigger a detonation in such a scenario. In particular, we concentrate on the possibility that the gradient mechanism would trigger a detonation on length scales that are under resolved or unresolved in our simulations, which corresponds to length scales $\lesssim 10$ km.

Much work has been done to determine the properties of the gradients required to successfully initiate a detonation by the Zel'dovich gradient mechanism (Arnett & Livne 1994; Niemeyer & Woosley 1997; Khokhlov et al. 1997; Röpke et al. 2007b; Seitzzahl et al. 2009b). Both Röpke et al. (2007b) and Seitzzahl et al. (2009b) studied systems initialized with a temperature gradient that included a constant density and composition (though the PGCD would also have a compositional gradient). Röpke et al. (2007b) examined the results of a linear temperature gradient. Seitzzahl et al. (2009b) performed a more comprehensive study with several functional forms for the temperature gradient and a wider range of conditions. The goal of the work was to determine the minimum size of the region containing the induction gradient for a self sustaining shock-reaction complex to form. This minimum size (or critical length scale, L_c) was determined to be a function of the input parameters of the system such as the ambient temperature, ambient density, peak temperature, steepness and functional form of the temperature profile, and composition of the fuel. In general, they find that for $L_c \lesssim 10$ km, a

composition of 50%-50% ^{12}C and ^{16}O with densities $\gtrsim 1 \times 10^7 \text{ g/cm}^3$ and peak temperatures $\gtrsim 2 \times 10^9 \text{ K}$ would successfully trigger a detonation.

Seitenzahl et al. (2009b) performed a resolution study on one of their models and examined how L_c changed when they increased their resolution. In this study, the L_c grew from $\sim 400 \text{ m}$ in the lowest resolution case to $\sim 1,000 \text{ m}$ in the highest resolution case (see their table 3). The grid resolution with which they ran their simulations may increase L_c for a given parameter set, or said another way, the grid resolution will increase the critical conditions required to trigger a detonation for a particular L_c . Because they only performed the resolution study on one set of parameters it is difficult to assess how much the critical conditions would increase with adequate resolution for a given L_c .

Seitenzahl et al. (2009b) also examined the conditions for the formation of a detonation for systems comprised of less than 50% ^{12}C by mass. In their most extreme case of carbon-poor fuel (30/70 C/O ratio) the critical radius is roughly a factor of 10 larger than fuel composed of equal amounts of carbon and oxygen. In general, the reduction of ^{12}C increased the critical length scale (their tables 8 - 11). They also tested the effect of adding ^4He (14% by mass) to the composition. The addition of helium dramatically decreased the critical length scale (their table 12). As with the resolution study, they only examined one set of parameters for their composition study, and thus did not determine how changing the composition with a fixed L_c would change the values of peak temperature, density, etc., required for a successful detonation. We note that by lowering the ^{12}C mass, the critical conditions would most likely increase, and for extremely carbon-poor environments a detonation may not be triggered at all. For the remainder of this work we assume that extremely carbon-poor environments are not encountered and that small to moderate deviations from a 50/50 C/O ratio would not substantially increase the critical temperature and density — at least to within the context of our approximation.

Khokhlov et al. (1997) examined the conditions under which the Zel'dovich gradient mechanism would produce a detonation given a gradient in both temperature and composition. They study two cases: In the first case turbulence tears apart an active flame and mixes cold fuel with hot ash to achieve the necessary conditions to initiate a detonation. In the second case, stellar expansion extinguishes the active flame allowing the hot ash and cold fuel to mix. As the star contracts, it squeezes the mixture - creating the necessary conditions for the mixture to detonate.

Khokhlov et al. (1997) argue that mixing is important in order for fuel to attain a high enough temperature to ignite at relatively low densities. They point out that cold fuel that obeys a WD equation of state would have to be compressed to $\approx 1 \times 10^{10} \text{ g/cm}^3$ in order to obtain a high enough temperature to ignite; however, mixing hot ash at a level as low as 10% raises the entropy enough that the mixture would ignite at densities $\approx 10^7 \text{ g/cm}^3$. Their figure 2 shows the critical density for ignition as a function of fuel mass fraction in the mixture.

In Khokhlov et al. (1997), a temperature gradient is set up in the mixing layer between cold fuel and hot ash.

The temperature of the mixture is low in regions dominated by fuel and is high in regions dominated by ash. It is thus a matter of compressing the mixture to the critical density (and thus the critical peak temperature through compressional heating) for a detonation to initiate in the mixture. Their Figure 6 shows L_c as a function of critical density for a gas initialized with a linear compositional gradient and a temperature gradient determined by the amount of ash in the mixture at a particular location. They conclude that in the WD environment, a detonation is possible for densities between $5 \times 10^6 \text{ g/cm}^3$ and $2 - 5 \times 10^7 \text{ g/cm}^3$. For a mixing layer with a critical length scale on the order of 10 km, the critical density of the fuel is $\approx 1 \times 10^7 \text{ g/cm}^3$. Interestingly, this is commensurate with the results of Seitenzahl et al. (2009b) with a 50/50 C-O composition, even though the two approaches were distinct.

We therefore conclude that for $L_c \approx 10 \text{ km}$, the critical density, $\rho \gtrsim 1 \times 10^7 \text{ g/cm}^3$ and with a corresponding critical peak temperature, $T \gtrsim 2 \times 10^9 \text{ K}$ are the necessary criteria to successfully trigger a detonation on that length scale. We remind the reader that we have assumed that the environment is not carbon-poor and that a decrease in the fuel mass will not dramatically increase the critical conditions. We have further assumed that though the method used to determine the critical values was unresolved, the results of a fully resolved study would not dramatically increase the critical values from the unresolved case. Though both the composition effects and uncertainties with the resolution of the method will affect the values critical for detonation, the values of temperature and density that we have selected are acceptable for our level of approximation.

3.1.2. Discussion of Mixing at the Fuel-Ash Interface

The PGCD detonates in the same manner as the second case described in Khokhlov et al. (1997), which depends on the formation of a fuel-ash mixture. In the PGCD, ash ejected from the star flows over the surface to the collision region. As the ash flows, it turbulently mixes with fuel on the surface forming a mixing layer of fuel and ash. In the following we demonstrate the feasibility of our mixing assumption by examining the growth of Kelvin-Helmholtz modes at the fuel-ash interface and showing that these modes can grow quickly enough and on the relevant length scales to provide the appropriate mixing. However, mixing is a complicated process and our assumptions below of constant physical conditions are meant to provide an order-of-magnitude estimates. We are particularly interested in the growth of the mixing layer on unresolved scales. As above, our length scale of interest is $L_c \approx 10 \text{ km}$.

Using typical values from the conditions present at the surface-ash interface, we can approximate the largest unstable Kelvin-Helmholtz length scale, λ_{max} , such that all $\lambda \leq \lambda_{max}$ would grow due to the instability. Using linear stability analysis, the largest unstable length scale is expressed in terms of the physical conditions at the interface between the flowing ash and the surface of the WD as

$$\lambda_{max} = \frac{2\pi \cdot \alpha_{fuel} \alpha_{ash} U^2}{g(\alpha_{fuel} - \alpha_{ash})}, \quad (1)$$

where $\alpha_{fuel} = \frac{\rho_{fuel}}{\rho_{fuel} + \rho_{ash}}$, $\alpha_{ash} = \frac{\rho_{ash}}{\rho_{fuel} + \rho_{ash}}$, ρ_{fuel} is

the fuel density (i.e. the surface density of the WD), ρ_{ash} is the ash density, $g \approx 1 \times 10^9 \text{ cm/s}^2$ is the acceleration due to gravity, and U is the velocity of the ash (Chandrasekhar 1961). The ash flows at a speed $U \approx 5 \times 10^8 \text{ cm/s}$ and the interface is located at $r_{interface} \approx 5 \times 10^8 \text{ cm}$ from the center of the star. Values for the densities are $\rho_{fuel} \approx 1 \times 10^6 \text{ g/cm}^3$ and $\rho_{ash} \approx 1 \times 10^5 \text{ g/cm}^3$. Inserting these values into equation (1) gives $\lambda_{max} \approx 1.0 \times 10^8 \text{ cm}$ - comparable to the radius of the star and hence $\gg L_c$. Therefore a region the size of L_c would develop Kelvin-Helmholtz instabilities which would drive turbulent mixing.

The ash must flow approximately half way around the star to reach the collision region. Using the values of U and $r_{interface}$ we can approximate the time it would take for the ash to reach the collision region, τ_{ash} , as

$$\tau_{ash} = \frac{\pi \cdot r_{interface}}{U} \quad (2)$$

Therefore $\tau_{ash} \approx 1\text{s}$. Note that this is consistent with the results of our simulations discussed in section 5.3 and shown in figure 5.

The timescale for the growth of the unstable Kelvin-Helmholtz modes with length scale λ (Chandrasekhar 1961) in the linear regime is

$$\tau_{KH}(\lambda) = [g(2\pi/\lambda)(\alpha_{fuel} - \alpha_{ash}) - (2\pi/\lambda)^2 \alpha_{fuel} \alpha_{ash} U^2]^{-1/2}. \quad (3)$$

The growth time scale for a perturbation of length scale $\lambda = L_c \text{ km}$ is $\tau_{KH}(10\text{km}) \approx 1 \times 10^{-3} \text{ s}$. Since $\tau_{ash} \gg \tau_{KH}(10\text{km})$, perturbations of length scale L_c will grow for several (linear analysis) e-folding times before the ash reaches the collision region.

We again note that the conditions at the ash-star interface are not constant, especially since the star is expanding as the ash flows over the surface. However, given the short growth timescale ($\tau_{KH} \approx 1 \times 10^{-3} \text{ s}$) for $L_c = 10 \text{ km}$, if the above conditions exist for only a small fraction of the time that the ash is flowing over the surface then the requisite modes would grow and mixing would develop by the time the ash reaches the collision region.

We conclude that it is possible for the Zel'dovich mechanism to trigger a detonation in the mixed fuel-ash layer on length scales not adequately resolved in our simulation if the critical conditions are reached. The ash flows turbulently mix with fuel on the surface driven by Kelvin-Helmholtz instabilities. The mixing process produces the necessary thermal and compositional gradients and the increase in density of the mixture as it pushes into the star both accelerates the combustion and shrinks the critical length scale, L_c , required for the gradients.

3.2. Numerical Treatment of Detonation Trigger

To treat the detonation physics we have incorporated the numerical scheme used by Meakin et al. (2009) and Seitenzahl et al. (2009b) which we briefly describe in section 4 and which was not present in J08. To correctly capture the Zel'dovich mechanism in the simulation we would need to resolve the required gradients as well as the carbon burning length scales within those gradients. This is prohibitively expensive for 3D simulations and we do not accomplish it here. Thus the initiation of a detonation in our simulations is a process that is severely

under resolved. The finest resolution in our simulation does not allow us to follow the simulation on length scales of $\lesssim 10 \text{ km}$. In section 3.1 we estimate that if a gradient is characterized by a peak temperature, $T \gtrsim 2 \times 10^9 \text{ K}$ and density, $\rho \gtrsim 1 \times 10^7 \text{ g/cm}^3$ on length scales of 10 km then the necessary conditions exist to produce a gradient-triggered detonation. We further show that mixing could occur on length scales on the order of 10 km as the ash flows around the star. Thus we adopt the criteria that if a computational cell's temperature and density exceed those specified above, then the necessary conditions exist for a gradient-triggered detonation and we allow the cell to detonate.

Numerically, we trigger the detonation by allowing the $^{12}\text{C} - ^{12}\text{C}$ reaction to run away. When a computational cell reaches a high enough temperature and density such that the carbon burning reaction rate becomes extremely high, all of the fuel in the cell burns in a single computational time step. If there is enough fuel in the cell, this releases a tremendous amount of energy, which dramatically increases the temperature and pressure in the cell, and creates a shock with the neighboring cells. The shock propagates outwards from the cell and burns material in its wake, forming a detonation. This is akin to the direct initiation of a detonation by a blast wave. Since the initiation of the detonation is purely numerical in nature, we stress that it simply indicates that a computational cell has reached the necessary thermodynamic conditions for rapid carbon burning. However, the conditions for rapid carbon burning also coincide with the necessary (but not sufficient) conditions that we expect would enable the Zel'dovich mechanism to produce a detonation as outlined in section 3.1. We refer the reader to Meakin et al. (2009) and Seitenzahl et al. (2009b,a) for a discussion of the initiation of detonations in the context of numerical simulations.

In our description of the detonation mechanism, we appeal to the fact that the ash ejected from the WD will mix with fuel on the surface of the star as it flows; however, we do not treat mixing on unresolved scales. Mixing on small scales occurs by numerical diffusion. Though we do not capture the details of that mixing process, we fully expect the material to be well mixed as it flows around the star as postulated in section 3.1.

Finally, due to the above mentioned physical processes that are not included in our simulations, the physical quantities that make up the trends discuss in section 5 and listed in table 1 that are the results of the detonation should be taken with a grain of salt. These properties (such as the radius at which the detonation occurs for example) are the result of the time at which the numerical detonation is triggered and the state of the contracting WD at that time. Though the conditions for which the numerical detonation is triggered roughly coincides with those that are sufficient to trigger a gradient-induced detonation, by approximating the relevant physics the exact time and location of the detonation are uncertain. Altering the detonation time and location could change the physical properties resulting from the detonation. Nevertheless because of the correspondence between the conditions for the numerical detonation and that of the physical detonation, we expect the general trends presented in section 5 to hold while we acknowledge that there may be large uncertainties.

4. NUMERICAL METHODS

We use the Adaptive Mesh Refinement (AMR) FLASH application framework (Fryxell et al. 2000; Dubey et al. 2009) to perform the simulations presented in this paper. FLASH is a modular, component-based application code framework created to simulate compressible, reactive astrophysical flows. The framework supports multiple methods for managing the discretized simulation mesh, including the PARAMESH (Parallel Adaptive Mesh Refinement) library (MacNeice et al. 2000), which implements a block-structured adaptive grid.

FLASH includes a directionally split piecewise-parabolic method (PPM) solver (Colella & Woodward 1984) descended from the PROMETHEUS code (Arnett et al. 1989). It has been successfully applied to a wide variety of large-scale terrestrial and astrophysical flow problems, ranging from simulations of homogeneous, isotropic turbulence (Benzi et al. 2008; Arnèodo et al. 2008), Raleigh-Taylor instability (Calder et al. 2002), shock-cylinder interaction (Weirs et al. 2005), and laser-driven high energy density laboratory experiments (Kane et al. 2001), to buoyancy-driven turbulent combustion (Townesley et al. 2008), wind-driven instabilities in neutron star atmospheres (Alexakis et al. 2004), contact binary stellar evolution (Ricker & Taam 2008), Type Ia supernovae (Jordan et al. 2008; Meakin et al. 2009; Jordan et al. 2009), galaxy collisions (Zuhone et al. 2008), and cosmological simulations of large-scale structure formation (Heitmann et al. 2005).

The energetics scheme employed to treat flames and detonation waves in our simulations uses three progress variables to track carbon burning, QSE relaxation, and NSE relaxation. Details concerning the nuclear physics and the numerical implementation are presented in Calder et al. (2007); Townesley et al. (2007) and Seitenzahl et al. (2009c). Subsonic burning fronts (deflagrations) are advanced using an advection-diffusion-reaction (ADR) equation. Details concerning the implementation, calibration and noise properties of the flame treatment can be found in Townesley et al. (2007) and references therein. Detonations are handled naturally by the reactive hydrodynamics solver in FLASH without the need for a front tracker. This approach is possible because unresolved Chapman-Jouguet (CJ) detonations retain the correct jump conditions and propagation speeds. Cellular structure smaller than the grid scale will be suppressed in our simulations but is free to form on resolved scales. The impact of cellular structure on the global evolution of the model is still uncertain; however, since cellular structure alters the detonation wave speed by only a few percent for the conditions being modeled (Timmes et al. 2000), the effect is likely to be small. Additional details related to the treatment of detonation waves are discussed in Meakin et al. (2009).

Self gravity is calculated by expanding the mass density field in multipole moments, which are used to approximate the scalar gravitational potential. The gravitational acceleration is calculated by approximating the derivative of the scalar potential at each location in the domain. The Helmholtz equation of state of Timmes & Swesty (2000) is used to describe the thermodynamic properties of the stellar plasma, including

contributions from blackbody radiation, ions, and electrons of an arbitrary degree of degeneracy.

5. SIMULATIONS AND RESULTS

5.1. Simulation Setup

We extended the study of the GCD model described in J08 with two primary differences. First, we included detonation physics in the simulations (as we described in sections 3.2 and 4) and followed the models from ignition, through the detonation phase, and to the free expansion phase. We terminated the simulations when the temperature decreases to the point that nuclear reactions ceased. Second, we initiated these simulations with multiple ignition points (as described in section 2.3) instead of a single ignition point with the method used in J08. For completeness we give the basic points here but refer the reader to J08 and references therein for more details.

Our simulations used FLASH’s AMR capabilities with a finest resolution of 8km. Each simulation contained a $1.365 M_{\odot}$ WD in hydrostatic equilibrium composed of equal parts carbon and oxygen. The WD had a central density of $2.2 \times 10^9 \text{ g/cm}^3$, an ambient temperature of $3 \times 10^7 \text{ K}$, a radius of approximately 2000 km, and a binding energy of $4.9 \times 10^{50} \text{ ergs}$. Although the core of the star is most likely convective with a turbulent convective RMS velocity $v_{\text{RMS}} \sim 16 \text{ km/s}$ (Nonaka et al. 2012), the turbulent convective RMS velocity is much less than the laminar flame speed, and so we have ignored the background convective turbulence, and initialized the star with zero velocity.

We initiated this series of simulations with multiple ignition “points”, which are 16 km spheres comprised of hot ash placed in the star at rest. We placed the ignition points in a spherical region whose center coincided with the z-axis. We parameterized the spherical region by its radius and z-offset (the distance from the origin of the center of the spherical region along the z-axis). The radius of the spherical region was 128 km and the z-offsets were 68 km, 88 km, and 168 km - one z-offset for each of our three simulations. We randomly populated a 128 km spherical region with 63 ignition points. We placed ignition points so that they did not overlap with one another, and so that they were contained entirely within the spherical region. We used the same random distribution of ignition points for all three simulations; they only differed by their relative location along the z-axis. Table 1 contains labels for the simulations referred to in this work along with parameters for the initial conditions.

5.2. Evolution of Simulations

In this section we describe the evolution of the PGCD model as demonstrated by the $63n128r168z$ simulation. Figures 1 and 2 show snapshots of the $63n128r168z$ simulation starting with the initial conditions and ending with the passage of the detonation wave. The green contour in the figures approximates the location of the WD’s surface. The orange regions are high temperature regions. These regions are primarily hot ash. The temperature ranges from $1 \times 10^9 \text{ K}$ (dark orange) to $5 \times 10^9 \text{ K}$ (bright orange).

Each simulation begins with one of the above multiple ignition point configurations. Panel (a) of Figure 1

shows the initial conditions of the *63n128r168z* simulation. In the first few tenths of a second, each ignition point quickly burns radially outward from its center and merges with the other ignition points to form a large asymmetric bubble of ash. The ash in the bubble is less dense than the surrounding stellar material and is therefore buoyant. After 0.3-0.4 seconds, the bubble, which continues to grow in size, begins to quickly rise towards the WD's surface. During the rise, Rayleigh-Taylor instabilities grow on the flame surface, which further increases the surface's complexity and enhances the burning rate (Khokhlov 1995; Townsley et al. 2008).

Panel (b) of Figure 1 shows the simulation at 0.6s. This panel shows the ignition points after they have risen and merged to form a complex volume whose surface has been enhanced by fluid instabilities.

After approximately 1.5 s, the rising ash bubble breaks through the stellar surface and begins spreading laterally across the star in all directions, converging on a region antipodal to the bubble breakout region. Since the density of the surface layers of the star are too low to maintain thermonuclear combustion, the flame quenches and the deflagration subsides. As the ash flows over the surface of the star, cold fuel (C and O) mixes with the ash at the interface between the ash and the stellar surface, creating a fuel-ash mixture.

Panels (c), (d), and (e) of Figure 1 are at 1.1 s, 1.4 s, and 1.9 s, respectively. These panels show the ash after it has broken out of the surface and has started to spread. In panel (c) the ash has spread approximately half way around the star. By 1.4 s (panel d), the ash has made it three-fourths the way around the star, and at 1.9 s (panel e) the ash has almost completely engulfed the WD.

A significant amount of nuclear energy, 1.9×10^{50} ergs (comparable to the binding energy of the WD), is released during the deflagration. This provides a kick to the star which causes it to expand. During the first few seconds, while the ash flows over the surface, the star expands to several times its original size. The expanding star slows the ash before it reaches the collision region. This shown in panels (c) - (f) of Figure 1 and panel (a) of Figure 2.

Panel (f) of Figure 1 is at 2.2 s and panel (a) of Figure 2 is at 2.5 s. The ash seems to disappear from the panels because the star has expanded and the ash has cooled to the point that it has fallen out of the color range. Panel (b) of Figure 2 is at 3.1 s. The WD is maximally expanded in this image.

Several seconds after the ash is ejected from the surface of the star, it converges at the opposite pole from where it broke out. The converging flow compresses the material in the collision region until the pressure is sufficient to stop the mixture from flowing laterally and to drive a plume of fuel and ash towards the interior of the star. Additionally, after the star has reached its maximally expanded state, it begins to contract. The stellar contraction increases the global density structure of the star, and thus the local density of at the collision region, eventually resulting in explosive C and O burning. Once the conditions for detonation are met (as discussed in section 3.1) and the detonation is triggered (as discussed in section 3.2) the combustion immediately sweeps across the star in a few tenths of a second.

Panels (c) and (d) of Figure 2, at 3.7 s and 4.2 s respectively, show the star as it contracts. A hot region can be seen forming at the "bottom" of the star. This hot region is the result of the compressional heating of the mixture in the collision region from the work done by the contracting star as well as the material flows themselves. Panel (e) of Figure 2 is at 4.3 s and shows the simulation just after the initiation of the detonation wave. Panel (f) of Figure 2 shows the simulation at 4.4 s. The detonation wave has consumed about half of the star in just over 0.1 s.

The detonation wave transforms the WD into a super-heated remnant composed of material that has reached nuclear statistical equilibrium (NSE) in the core (which is dominated by iron-group elements, most of which is ^{56}Ni) surrounded by a layer of intermediate mass elements and topped off with the ash of partially burned C and O. This whole structure is shrouded by the products of the deflagration which consisted of iron-group elements, intermediate mass elements, carbon burning products, and unburned C and O. The super-heated structure quickly expands and cools, and is transitioning into a homologous structure when the simulations are stopped.

5.3. Results

In each of our simulations, we found the necessary conditions to trigger a detonation as discussed in section 3. The main properties of the three simulations are summarized in Table 1. The simulations differ in the location of the center of their sphere of ignition points, and are labeled *63n128r68z* (ignition sphere centered 68 km from the center of the star), *63n128r88z* (88 km from the center of the star), and *63n128r168z* (168 km from the center of the star).

The deflagration phase of the SN Ia provides a kick to the WD which causes the WD to rapidly expand and then contract. It is the expansion and subsequent detonation on contraction that characterizes the pulsation GCD model. Figure 3 shows the amount of nuclear energy release as a fraction of the binding energy of the star as a function of time for the three simulations. The simulations trend together for the first 0.8s and then diverged. The deflagration continued to release nuclear energy until approximately 1.5s in each simulation, at which time the flame stopped burning. In general, the simulations whose ignition points were placed closer to the core of the WD burned more during the deflagration and thus imparted more energy to the star. The amount of energy released ranged from 18.9×10^{49} ergs to 38.6×10^{49} ergs, or between 38% and 78% of the binding energy of the star. By comparison, the single bubble initial conditions in J08 released between 3.0×10^{49} ergs and 10.5×10^{49} ergs, or between 6% and 21% of the binding energy of the WD.

The energy released during the deflagration phase was sufficient to cause the star to undergo an energetic pulsation. Figure 4 shows the evolution of the maximum density found in the computational domain, which is equivalent to the central density of the WD (prior to detonation) for the three simulations and gives a measure of the strength and the period of the pulsation. In each simulation, the WD expanded to a maximum amplitude and then contracted before detonating. The simulation that expanded the least was *63n128r168z*

which reached a minimum central density, $\rho_{c,min}$, of $3.51 \times 10^7 \text{ g/cm}^3$. The star expanded for 3.1 s before it began to contract. By contrast, *63n128r68z* achieved $\rho_{c,min} = 0.43 \times 10^7 \text{ g/cm}^3$, and the WD did not begin to contract until 4.71 s. Thus the more energy released during the deflagration phase, the more the WD expands and the longer its pulsational period. The vertical lines in Figure 4 mark the time at which the star detonates.

As the WD expanded, ash was ejected from the surface and flowed laterally over the star, mixing with surface fuel as it flowed. Figure 5 plots the polar angle of the leading edge of the flow as a function of time. Initially a small region of ash crossed the origin and was responsible for the large values of θ seen in the figure during the first second. After one second, the ash reached the surface and started to spread around the star. The ash, which mixes with fuel on the surface as it flows, quickly reached a polar angle of approximately 150° and then stalled in each of the simulations. This was in part because the mixture pushed some material in front of it which compressed material in the collision region and increased the pressure there. Also, the expansion of the star robbed kinetic energy from the flow which also contributed to the mixture stalling. Once the star contracted, the mixture slowly pushed its way further around the star, as well as into the high density regions towards the core. As before, the lines on the graph highlight the time at which the star detonated. The mixture only stalled for a short period of time in the *63n128r168z* simulation whose WD had the shortest pulsational period. The opposite is true for the *63n128r68z* simulation in which the mixture stalled the longest and the WD had the longest pulsational period. Even though the mixture encroached on the collision region within a few seconds from when the flow started, it was the contraction of the star that assisted the mixture in making the final move to higher densities.

After the star began to contract, the fuel-ash mixture made its way into the high-density layers of the WD. Figure 6 shows the evolution of the thermodynamic conditions in the fuel-ash mixture as it pushed into the star. The top plot in figure 6 shows the temperature of the computational cell with the maximum temperature in the mixture. The middle plot shows the density and the bottom plot shows the radius of the computational cell with the maximum temperature. Both the temperature and density follow the trend of the central density, as the WD expanded and contracted. As the star expanded, the temperature and density of the mixture decreased. As the star contracted, the temperature and density of the mixture increased. The location of the hot spot followed the same pattern; hence, as the star contracted, the radius of the hot spot moves closer to the core. This was due both to the stellar contraction and the continued flow of the mixture. Once the temperature of the hot spot exceeded $\sim 2.0 \times 10^9 \text{ K}$ and the density exceeded $\sim 1 \times 10^7 \text{ g/cm}^3$ rapid combustion ensued, which transitioned into a detonation. We stress that the detonation is the result of the numerical scheme discussed in section 3.2 and is not the result of the Zel'dovich gradient mechanism. It merely indicates that the conditions in the computational cell surpass those that are necessary to produce a gradient-induced detonation. In the *63n128r168z* simulation, the deflagration phase released

the least amount of energy of all the simulations and thus the WD expanded the least, it had a shortest pulsational period, it began contracting the earliest. As a result, the detonation occurred the soonest. The opposite is true for the *63n128r68z* simulation whose deflagration phase released the most amount of energy and whose detonation was triggered last.

An important set of observables of an SN Ia are the nucleosynthetic yields produced in the event. We have approximated the yields from the three models using the reaction progress variables from FLASH's burning module (Calder et al. 2007). Table 2 lists the post-explosion nucleosynthetic yields from our simulations in terms of the quasi-static equilibrium groups that are represented by the progress variables. Note that the material that burned to NSE is predominately iron-group elements, most of which is ^{56}Ni . Thus, the amount of NSE material can be considered an upper limit on the amount of ^{56}Ni produced during the explosion. The upper limit on the ^{56}Ni produced during these simulations ranges from $\sim 1.0 M_\odot$ to $\sim 0.7 M_\odot$. Though yields of $\sim 1.0 M_\odot$ of ^{56}Ni are associated with luminous SNe Ia, yields of $\sim 0.7 M_\odot$ of ^{56}Ni are associated with SNe Ia of normal luminosity. The combined mass of the intermediate mass elements and NSE material is $1.1 M_\odot$ and is consistent with observed SNe Ia (Mazzali et al. 2007).

The deflagration phase of the PGCD models burns approximately $0.1 - 0.25 M_\odot$ of material. This material is ejected into the outer regions of the system, surrounding the WD when it detonates. Table 3 lists the nucleosynthetic yields produced during the deflagration phase of the three simulations. The primary product of the deflagration phase is NSE material with about a third of the material composed of carbon burning products and intermediate mass elements.

These simulations show that through the course of an off-centered ignition, if a detonation is not triggered as the flame breaks down when it moves through the low density layers of the star on its way to the surface (i.e. the first scenario in (Khokhlov et al. 1997)) and if the energy release during the deflagration is sufficient to significantly disrupt the star and cause it to rapidly expand, ash will flow around the surface (mixing with cold fuel as it flows), and stall in the collision region while the star is expanding. As the WD contracts, the conditions in the fuel-ash mixture are pushed to higher temperature and density until the values exceed that which are necessary to produce a gradient-triggered detonation. Once the detonation is triggered in the mixture, it quickly consumes the star.

6. COMPARISON OF DETONATION MECHANISM TO PREVIOUS GCD MODELS

The classical GCD model of SNe Ia is postulated to be possible if the energy released during the deflagration phase does not significantly expand the star. With little stellar expansion, the fuel density in the collision region is high enough for compression by the in-flowing ash to increase the temperature in the fuel and ultimately initiate a detonation. For the purposes of demonstrating this, we restarted the *16b100o8r* simulation from J08 just prior to detonation with the detonation physics included in simulation. Figure 7 shows the evolution of the *16b100o8r* classical GCD model leading up to the detonation. The

top left panel of the figure is at $t=1.8$ s. It shows the ash as it approached the collision region. Fuel pushed ahead of the ash increased in temperature due to compressional heating. This hot region formed a jet that flowed both towards and away from the surface of the star. The top right panel is at $t=1.9$ s. The ash converged further into the collision region. The hot fuel continued to increase in temperature and had begun to slowly burn carbon as a result. This smoldering also increased the fuel temperature. The bottom left panel is at $t=2.22$ s. At this time the ash flows have collided. The hot fuel has further increased in temperature due to further compressional heating and due to combustion. The head of the hot jet has pushed the high temperature region and has reached the higher density layers of the white dwarf. The sufficient thermodynamic conditions to produce a detonation have been met and a detonation was triggered in the hot smoldering material. The formation of the detonation can be seen at the head of the hot jet. Finally, the bottom right panel at $t=2.3$ s shows the simulation after the detonation occurred. The detonation wave is propagating outward from its initiation point. The high temperature region behind the detonation as well as the smooth detonation front is visible in this image.

The PGCD model of SNe Ia is possible if the deflagration phase releases enough energy to cause the WD to expand significantly, but not so much energy that the star becomes unbound. Figure 8 shows the evolution of the PGCD model, $63n128r168z$, leading up to the detonation. The top left panel is at $t=3.5$ s where the mixture was beginning to approach the collision region. In contrast to the classical GCD, the ash flows and collision region were at low densities and no significant compressional heating of the fuel in the collision region occurred. The top right panel is at $t=3.8$ s. Note that this panel is zoomed with respect to the previous panel. The fuel-ash mixture continued to push into the collision region. The mixture began to heat since the WD was contracting and the ash was pushing to higher densities towards the core of the WD. The bottom left panel is at $t=4.1$ s. Note that this panel is again zoomed in from the previous panel. The WD has continued to contract and the mixture continued to move to higher densities. The mixture heated significantly due to 1) compressional heating from the mixture pushing to higher densities and from the WD contracting and 2) the mixture reaching conditions that caused it to smolder. The mixture then approached the critical density above which a detonation would be initiated. The bottom left panel is at 4.22 s Note that, again, this panel is zoomed in from the previous panel. The mixture reached the necessary thermodynamic conditions for a gradient-triggered detonation. The detonation was triggered in the simulation as described in section 3.2. Two detonation waves can be seen emerging from the mixture layer in the image. The bottom right panel is at $t=4.3$ s. The detonation is propagating outward from its initiation point through the star. The high temperature region behind the detonation wave as well as the smooth detonation front are clearly visible.

In summary, the classical GCD model detonates as the WD is expanding. The thermodynamic conditions for detonation are reached when the ash flows compress and heat fuel in the collision region and force this hot fuel into the high density layers of the star. In contrast, the PGCD

model detonates as the WD contracts. The thermodynamic conditions for detonation are achieved by the combination of the contraction of the WD which increases the temperature and density of the fuel-ash mixture, as the mixture pushes its way towards the high density core of the WD.

7. DISCUSSION

7.1. *Properties of the PGCD Scenario*

7.1.1. *Comments on the Detonation Mechanism*

In the classical GCD model, flowing ash must compress fuel in the collision region to achieve the thermodynamic conditions necessary to launch a detonation. This would seem to require the ash flows to converge symmetrically so that they focus on a localized region. Thus far, the only successful classical GCD simulations have been performed in 2D cylindrical geometry ((Meakin et al. 2009) for example) which imposes azimuthal symmetry, and in 3D with single bubble ignition points as initial conditions which, by their nature, evolve in an azimuthally symmetric manner. Our PGCD models were initiated with multiple ignition points. These ignition points evolved into an asymmetric volume of ash which produced asymmetric ash flows on the surface. However, the PGCD depends less stringently on the details of the ash flows. As long as the mixture is redirected towards the core of the star, the contraction of the WD will do the rest, even if the flow lacks symmetry. As a result, the PGCD model, in principle, is a more robust detonation mechanism compare to the classical GCD scenario in that it only depends on getting the fuel-ash mixture to a high enough density as the star contracts.

7.1.2. *Nucleosynthesis*

For any SN Ia model, the luminosity of the model is strongly related to the amount of ^{56}Ni produced in the explosion. This depends in turn on the density of the plasma before it is burned. A fair rule of thumb is that if $\rho \gtrsim 1.0 \times 10^7 \text{ g/cm}^3$ then that material will burn to NSE, which is predominantly iron-group elements comprised mostly of ^{56}Ni (see e.g., the comparison made in figure 12 of Meakin et al. (2009) and the discussion in their Section 5). The WD in the PGCD model is contracting from an expanded state when it detonates. As a result, there is a reduced amount of high density material. It is therefore in principle possible for the model to produce range of abundances of ^{56}Ni - and thus of luminosities - depending on the expanded state of the WD when it detonates.

The classical GCD models described in J08 detonate as the WD is expanding after a weak deflagration phase. The star is still fairly compact and there is ample high density material when the star detonates. The amount of ^{56}Ni produced in each of those models is greater than $1 M_{\odot}$ which corresponds to overly luminous SNe Ia. By contrast, the PGCD model is more easily able to access regions in model space that correspond to the $0.7 M_{\odot}$ values of ^{56}Ni production — typical of normal SNe Ia. Furthermore, the production of intermediate mass elements between the two scenarios is comparable. The classical GCD models in J08 produced between $0.1 M_{\odot}$ to $0.36 M_{\odot}$ of intermediate mass elements whereas the PGCD produces between $0.22 M_{\odot}$ and $0.33 M_{\odot}$ of inter-

mediate mass elements when adding the contributions of ^{24}Mg and Si-group elements.

7.1.3. *Observational Features of the Pulsational GCD Model*

The PGCD model has a post detonation geometry similar to the classical GCD model. The explosion is the result of a single off-centered detonation. The location of the detonation is at the antipodal point from where the star ejected the ash from its interior. This confers approximate azimuthal symmetry upon the system. The degree of asymmetry is determined in part by the radial offset of the detonation trigger. The larger the offset, the higher degree of asymmetry. We list the radial offset of the detonation location in our simulations in table 1.

In the PGCD model, the star detonates after the cessation of the deflagration phase. There is no active flame in the interior of the star at the time of detonation and thus no compositional inhomogeneities from deflagration ash. When the detonation occurs, it produces a smooth interior of NSE material surrounded by a layer of intermediate mass elements. The intermediate mass elements are surrounded by a shroud of ash produced in the deflagration, which is a mixture of intermediate mass elements and NSE material. This would suggest that elements, such as Fe, would be present in the high-velocity, outer layers of the ejecta and appear as such in the spectra. The flow of this ash over the surface of the WD produces a clumpy, choppy outer boundary to the intermediate mass element layer of the remnant. This is similar to structure suggested by the spectropolarimetry measurements of Wang et al. (2006, 2007). Furthermore, very early spectra taken at ~ 1 day after the explosion from the SN Ia 2011fe show that there is O, Mg, Si, S, Ca, and Fe - which are products of the deflagration in our models - in the outer most layers of the remnant (Nugent et al. 2011). Finally, table 1 lists the post explosion kinetic energy for the three simulations. These energies are $\sim 1 \times 10^{51}$ ergs and are consistent with observations of SNe Ia.

7.2. *Comparison to Other Work*

It is interesting to compare our results to the results from the 3D simulations in Röpke et al. (2007b). They initialize their simulations with a single spherical bubble, a region of small bubbles emulating a single bubble with surface perturbations, and a configuration of bubbles confined to a tear-drop-shaped envelope. Of the six 3D simulations they performed, two of the WDs in the simulation became unbound due to the energy released during the deflagration phase. Of the four simulations in which the WD remained bound, the deflagration energy release was in the range of $1 \times 10^{50} - 3.3 \times 10^{50}$ ergs, or roughly $\sim 20\% - 60\%$ of the binding energy of the WD. Furthermore, one of their single-bubble ignition model released 2.79×10^{50} ergs — comparable to our 63n128r88z simulation (their other single bubble ignition model disrupted the star). These values of the energy released during the deflagration phase are similar to those presented in our work. They found that the conditions for detonation are not reached in any of their simulations; however, they stopped their simulations when the conditions for deto-

nation are not met in the scenario presented in J08. The further evolution of their simulations would have been interesting in light of the results presented here.

8. CONCLUSION

We have conducted a series of numerical experiments simulating the evolution of a WD star in which we initiate a deflagration at off-center ignition points. The amount of energy released during the deflagration phase is enough to cause the star to undergo an energetic pulsation. As in the classical GCD model, the off-center ignition leads to a plume of material that is ejected from the star, flows laterally over the stellar surface, and converges on a collision region at the antipodal point from the ash breakout point. As the WD contracts, it creates thermodynamic conditions in the collision region such that it is possible for the Zel'dovich gradient mechanism to trigger a detonation. We find that these necessary (but not sufficient) conditions for detonation are reached in all three of our models. The energy deposition from the deflagration phase in these models ranges from 38% to 78% of the binding energy of the WD. We further comment that the detonation mechanism in the PGCD depends only on the bulk fluid motion of the system after the deflagration is ignited as opposed to a specific flow pattern, such as the focusing of the ash flows in the collision region in the classical GCD. This property confers a measure of robustness to the detonation mechanism.

Finally, the features of the PGCD qualitatively agree with the observations of SNe Ia, insofar as such comparisons can be made without subjecting the remnant to a radiation transfer treatment in order to compute actual light curves. The three models produced upper limits on the yields of ^{56}Ni ranging from $0.72 M_{\odot}$ to $0.98 M_{\odot}$. These ^{56}Ni yields are less than those produced in the classical GCD models of J08, primarily because the WD in our models is in a more expanded state at the time of detonation and contains a lower abundance of high-density, NSE-producing matter. This class of models allows SNe Ia to evolve and detonate with characteristics similar to the classical GCD while producing supernovae of lower luminosity.

The authors thank the FLASH Code Group, especially Chris Daley and Anshu Dubey for help with the development of and troubleshooting the code. We thank Brad Gallagher for creating figures 1 and 2. We also thank Katherine Riley, Mike Papka, and the staff at the Argonne Leadership Computing Facility at Argonne National Laboratory for help running our large-scale simulations on Intrepid at ANL. This work was supported in part at the University of Chicago by the U.S Department of Energy (DOE) under Contract B523820 to the ASC Alliances Center for Astrophysical Nuclear Flashes, and in part by the National Science Foundation under Grant No. AST - 0909132 for the ‘‘Petascale Computing of Thermonuclear Supernova Explosions’’. This research used computational resources awarded under the INCITE program at ALCF at ANL, which is supported by the Office of Science of the US Department of Energy under Contract No. DE-AC02-06CH11357.

We dedicate this work to the memory of our colleague and dear friend, Nathan Hearn.

REFERENCES

- Alexakis, A., Calder, A. C., Heger, A., Brown, E. F., Dursi, L. J., Truran, J. W., Rosner, R., Lamb, D. Q., Timmes, F. X., Fryxell, B., Zingale, M., Ricker, P. M., & Olson, K. 2004, *ApJ*, 602, 931
- Arnóodo, A., Benzi, R., Berg, J., Biferale, L., Bodenschatz, E., Busse, A., Calzavarini, E., Castaing, B., Cencini, M., Chevillard, L., Fisher, R. T., Grauer, R., Homann, H., Lamb, D., Lanotte, A. S., Lévêque, E., Lüthi, B., Mann, J., Mordant, N., Müller, W., Ott, S., Ouellette, N. T., Pinton, J., Pope, S. B., Roux, S. G., Toschi, F., Xu, H., & Yeung, P. K. 2008, *Physical Review Letters*, 100, 254504
- Arnett, D., Fryxell, B., & Mueller, E. 1989, *ApJ*, 341, L63
- Arnett, D. & Livne, E. 1994, *ApJ*, 427, 330
- Benzi, R., Biferale, L., Fisher, R. T., Kadanoff, L. P., Lamb, D. Q., & Toschi, F. 2008, *Physical Review Letters*, 100, 234503
- Branch, D., Buta, R., Falk, S. W., McCall, M. L., Uomoto, A., Wheeler, J. C., Wills, B. J., & Sutherland, P. G. 1982, *ApJ*, 252, L61
- Bravo, E. & García-Senz, D. 2009, *ApJ*, 695, 1244
- Bravo, E., García-Senz, D., Cabezón, R. M., & Domínguez, I. 2009, *ApJ*, 695, 1257
- Calder, A. C., Fryxell, B., Plewa, T., Rosner, R., Dursi, L. J., Weirs, V. G., Dupont, T., Robey, H. F., Kane, J. O., Remington, B. A., Drake, R. P., Dimonte, G., Zingale, M., Timmes, F. X., Olson, K., Ricker, P., MacNeice, P., & Tufo, H. M. 2002, *ApJS*, 143, 201
- Calder, A. C., Townsley, D. M., Seitzzahl, I. R., Peng, F., Messer, O. E. B., Vladimirova, N., Brown, E. F., Truran, J. W., & Lamb, D. Q. 2007, *ApJ*, 656, 313
- Chandrasekhar, S. 1961, *Hydrodynamic and hydromagnetic stability*, ed. Chandrasekhar, S.
- Colella, P. & Woodward, P. R. 1984, *Journal of Computational Physics*, 54, 174
- Dark Energy Task Force.
2006, Report of the Dark Energy Task Force, Available online at http://www.nsf.gov/mps/ast/aaac/dark_energy_task_force/report/detf_sfnbsrprpt.pdf
- Dubey, A., Antypas, K., Ganapathy, M., Reid, L., Riley, K., Sheeler, D., Siegel, A., & Weide, K. 2009, *Parallel Computing*, 35, 512
- Fryxell, B., Olson, K., Ricker, P., Timmes, F. X., Zingale, M., Lamb, D. Q., MacNeice, P., Rosner, R., Truran, J. W., & Tufo, H. 2000, *ApJS*, 131, 273
- Gamezo, V. N., Khokhlov, A. M., & Oran, E. S. 2004, *Physical Review Letters*, 92, 211102
- . 2005, *ApJ*, 623, 337
- Heitmman, K., Ricker, P. M., Warren, M. S., & Habib, S. 2005, *ApJS*, 160, 28
- Iben, Jr., I. & Tutukov, A. V. 1984, *ApJS*, 54, 335
- Jordan, G. C., Meakin, C. A., Hearn, N., Fisher, R. T., Townsley, D. M., Lamb, D. Q., & Truran, J. W. 2009, in *Astronomical Society of the Pacific Conference Series*, Vol. 406, *Astronomical Society of the Pacific Conference Series*, ed. N. V. Pogorelov, E. Audit, P. Colella, & G. P. Zank, 92–+
- Jordan, IV, G. C., Fisher, R. T., Townsley, D. M., Calder, A. C., Graziani, C., Asida, S., Lamb, D. Q., & Truran, J. W. 2008, *ApJ*, 681, 1448
- Kane, J. O., Robey, H. F., Remington, B. A., Drake, R. P., Knauer, J., Ryutov, D. D., Louis, H., Teyssier, R., Hurricane, O., Arnett, D., Rosner, R., & Calder, A. 2001, *Phys. Rev. E*, 63, 055401
- Khokhlov, A. M. 1991, *A&A*, 245, 114
- . 1995, *ApJ*, 449, 695
- Khokhlov, A. M., Oran, E. S., & Wheeler, J. C. 1997, *ApJ*, 478, 678
- Kim, A., Linder, E., Miquel, R., & Mostek, N. 2004, *Monthly Notices of the Royal Astronomical Society*, 347, 909
- MacNeice, P., Olson, K. M., Mobarri, C., de Fainchtein, R., & Packer, C. 2000, *Computer Physics Communications*, 126, 330
- Maoz, D., Sharon, K., & Gal-Yam, A. 2010, *ApJ*, 722, 1879
- Mazzali, P. A., Röpke, F. K., Benetti, S., & Hillebrandt, W. 2007, *Science*, 315, 825
- Meakin, C. A., Seitzzahl, I., Townsley, D., Jordan, G. C., Truran, J., & Lamb, D. 2009, *ApJ*, 693, 1188
- Niemeyer, J. C. & Woosley, S. E. 1997, *ApJ*, 475, 740
- Nomoto, K. 1982, *ApJ*, 253, 798
- Nomoto, K. & Kondo, Y. 1991, *ApJ*, 367, L19
- Nomoto, K., Thielemann, F.-K., & Yokoi, K. 1984, *ApJ*, 286, 644
- Nonaka, A., Aspiden, A. J., Zingale, M., Almgren, A. S., Bell, J. B., & Woosley, S. E. 2012, *ApJ*, 745, 73
- Nugent, P. E., Sullivan, M., Cenko, S. B., Thomas, R. C., Kasen, D., Howell, D. A., Bersier, D., Bloom, J. S., Kulkarni, S. R., Kandrashoff, M. T., Filippenko, A. V., Silverman, J. M., Marcy, G. W., Howard, A. W., Isaacson, H. T., Maguire, K., Suzuki, N., Tarlton, J. E., Pan, Y.-C., Bildsten, L., Fulton, B. J., Parrent, J. T., Sand, D., Podsiadlowski, P., Bianco, F. B., Dilday, B., Graham, M. L., Lyman, J., James, P., Kasliwal, M. M., Law, N. M., Quimby, R. M., Hook, I. M., Walker, E. S., Mazzali, P., Pian, E., Ofek, E. O., Gal-Yam, A., & Poznanski, D. 2011, *Nature*, 480, 344
- Pakmor, R., Hachinger, S., Röpke, F. K., & Hillebrandt, W. 2011, *A&A*, 528, A117
- Pakmor, R., Kromer, M., Röpke, F. K., Sim, S. A., Ruitter, A. J., & Hillebrandt, W. 2010, *Nature*, 463, 61
- Perlmutter, S., Aldering, G., Goldhaber, G., Knop, R. A., Nugent, P., Castro, P. G., Deustua, S., Fabbro, S., Goobar, A., Groom, D. E., Hook, I. M., Kim, A. G., Kim, M. Y., Lee, J. C., Nunes, N. J., Pain, R., Pennypacker, C. R., Quimby, R., Lidman, C., Ellis, R. S., Irwin, M., McMahon, R. G., Ruiz-Lapuente, P., Walton, N., Schaefer, B., Boyle, B. J., Filippenko, A. V., Matheson, T., Fruchter, A. S., Panagia, N., Newberg, H. J. M., Couch, W. J., & The Supernova Cosmology Project. 1999, *ApJ*, 517, 565
- Phillips, M. M. 1993, *ApJ*, 413, L105
- Raskin, C., Timmes, F. X., Scannapieco, E., Diehl, S., & Fryer, C. 2009, *MNRAS*, 399, L156
- Ricker, P. M. & Taam, R. E. 2008, *ApJ*, 672, L41
- Riess, A. G., Filippenko, A. V., Challis, P., Clocchiatti, A., Diercks, A., Garnavich, P. M., Gilliland, R. L., Hogan, C. J., Jha, S., Kirshner, R. P., Leibundgut, B., Phillips, M. M., Reiss, D., Schmidt, B. P., Schommer, R. A., Smith, R. C., Spyromilio, D., Stubbs, R., Suntzeff, N. B., & Tonry, J. 1998, *AJ*, 116, 1009
- Röpke, F. K., Hillebrandt, W., Schmidt, W., Niemeyer, J. C., Blinnikov, S. I., & Mazzali, P. A. 2007a, *ApJ*, 668, 1132
- Röpke, F. K., Woosley, S. E., & Hillebrandt, W. 2007b, *ApJ*, 660, 1344
- Rosswog, S., Kasen, D., Guillochon, J., & Ramirez-Ruiz, E. 2009, *ApJ*, 705, L128
- Saio, H. & Nomoto, K. 1998, *ApJ*, 500, 388
- . 2004, *ApJ*, 615, 444
- Seitzzahl, I. R., Meakin, C. A., Lamb, D. Q., & Truran, J. W. 2009a, *ApJ*, 700, 642
- Seitzzahl, I. R., Meakin, C. A., Townsley, D. M., Lamb, D. Q., & Truran, J. W. 2009b, *ApJ*, 696, 515
- Seitzzahl, I. R., Townsley, D. M., Peng, F., & Truran, J. W. 2009c, *Atomic Data and Nuclear Data Tables*, 95, 96
- Shen, K. J., Bildsten, L., Kasen, D., & Quataert, E. 2011, *ArXiv e-prints*
- Timmes, F. X. & Swesty, F. D. 2000, *ApJS*, 126, 501
- Timmes, F. X., Zingale, M., Olson, K., Fryxell, B., Ricker, P., Calder, A. C., Dursi, L. J., Tufo, H., MacNeice, P., Truran, J. W., & Rosner, R. 2000, *ApJ*, 543, 938
- Townsley, D. M., Bair, R. A., Dubey, A., Fisher, R. T., Hearn, N. C., Lamb, D. Q., & Riley, K. M. 2008, *Journal of Physics Conference Series*, 125, 012009
- Townsley, D. M., Calder, A. C., Asida, S. M., Seitzzahl, I. R., Peng, F., Vladimirova, N., Lamb, D. Q., & Truran, J. W. 2007, *ApJ*, 668, 1118
- van Kerkwijk, M. H., Chang, P., & Justham, S. 2010, *ApJ*, 722, L157
- Wang, L., Baade, D., Höflich, P., Wheeler, J. C., Kawabata, K., Khokhlov, A., Nomoto, K., & Patat, F. 2006, *ApJ*, 653, 490
- Wang, L., Baade, D., & Patat, F. 2007, *Science*, 315, 212
- Webbink, R. F. 1984, *ApJ*, 277, 355
- Weirs, G., Dwarkadas, V., Plewa, T., Tomkins, C., & Marr-Lyon, M. 2005, *Ap&SS*, 298, 341
- Whelan, J. & Iben, Jr., I. 1973, *ApJ*, 186, 1007
- Zel'dovich, Y. B., Librovich, V. B., Makhviladze, G. M., & Sivashinskii, G. I. 1970, *Journal of Applied Mechanics and Technical Physics*, 11, 264

- Zhu, C., Chang, P., van Kerkwijk, M., & Wadsley, J. 2011, ArXiv e-prints
- Zingale, M., Nonaka, A., Almgren, A. S., Bell, J. B., Malone, C. M., & Woosley, S. E. 2011, ApJ, 740, 8
- ZuHone, J., Ricker, P., Lamb, D., & Yang, H. 2008, in Bulletin of the American Astronomical Society, Vol. 40, Bulletin of the American Astronomical Society, 219–+

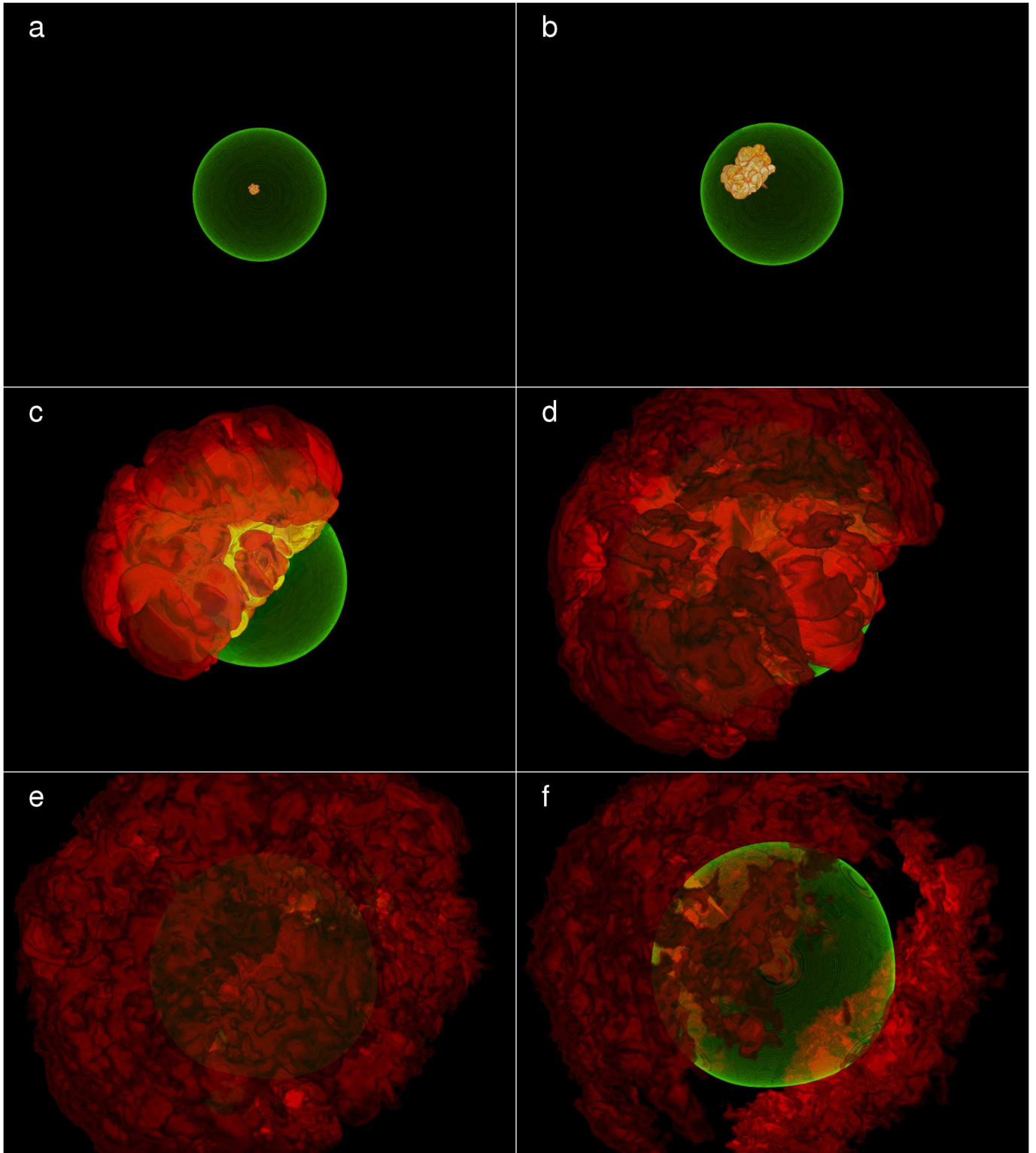


FIG. 1.— Six snapshots of the $63n128r168z$ simulation. The green contour approximates the location of the WD surface. The range of orange colors are regions of high temperature. Bright orange is at the top end of the scale at 5×10^9 K and dark orange is at the bottom at 1×10^9 K. The high temperature regions consist primarily hot ash. The simulation time associated with each panel is: (a) 0.0 s, (b) 0.6 s, (c) 1.1 s, (d) 1.4 s, (e) 1.9 s, and (f) 2.2 s. Further discussion of this figure can be found in section 5.2.

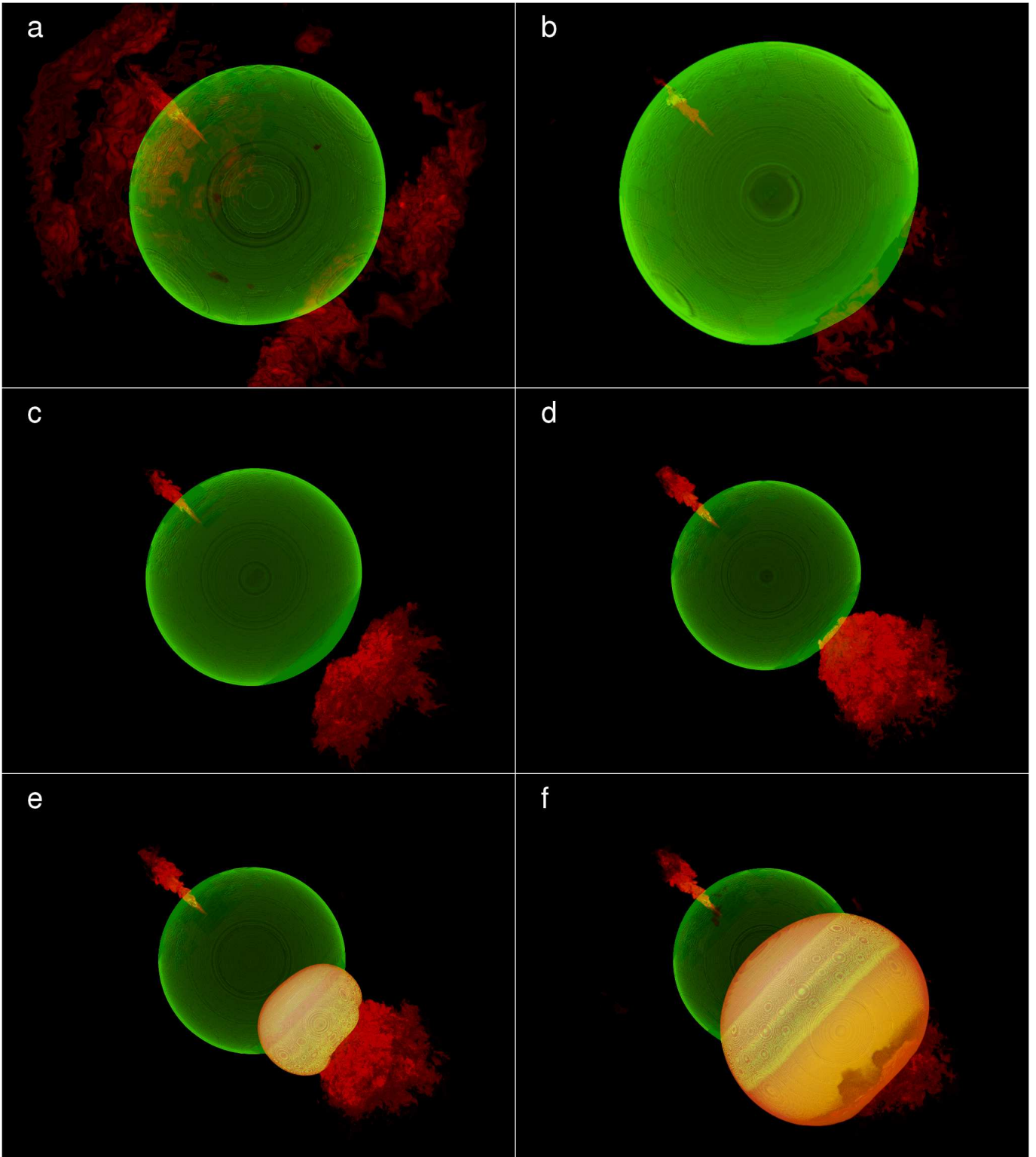


FIG. 2.— Six snapshots of the $63n128r168z$ simulation. The green contour approximates the location of the WD surface. The range of orange colors are regions of high temperature. Bright orange is at the top end of the scale at 5×10^9 K and dark orange is at the bottom at 1×10^9 K. The high temperature regions consist primarily hot ash. The simulation time associated with each panel is: (a) 2.5 s, (b) 3.1 s, (c) 3.7 s, (d) 4.2 s, (e) 4.3 s, and (f) 4.4 s. Further discussion of this figure can be found in section 5.2.

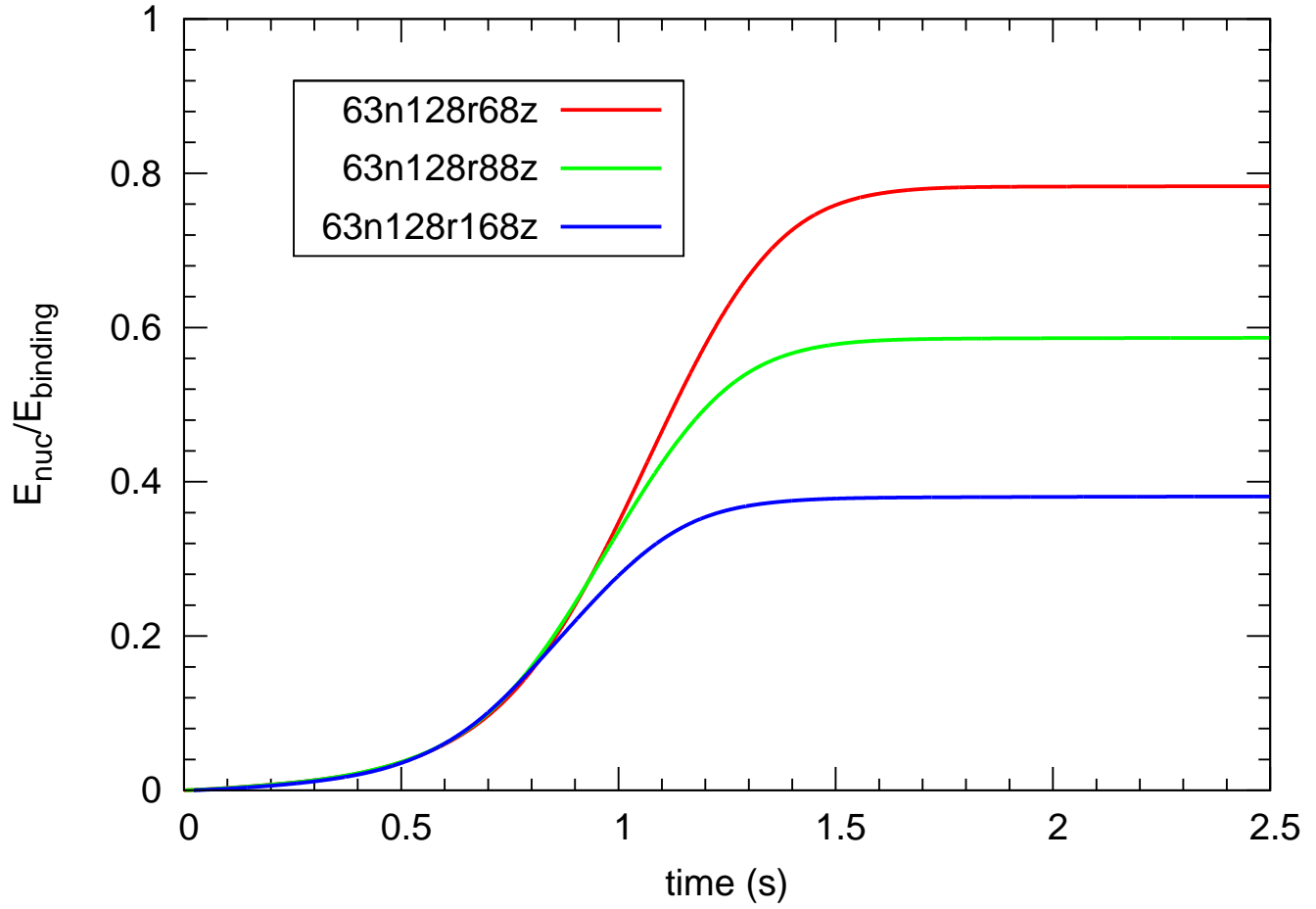


FIG. 3.— The fraction of binding energy increased due to nuclear energy input from the deflagration phase vs time for the three simulations.

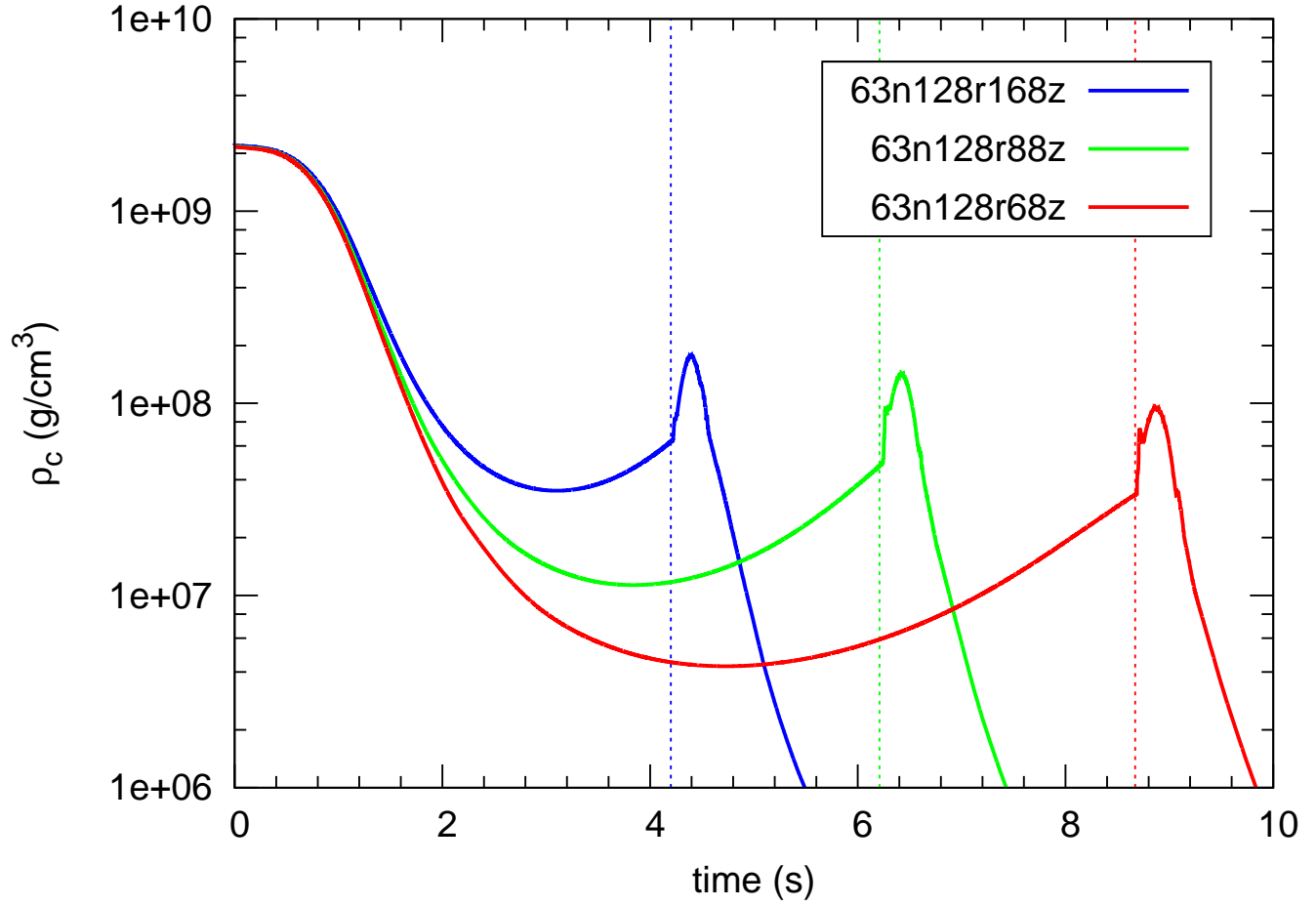


FIG. 4.— The maximum density in the computational domain (which corresponds to the central density, ρ_c , of the WD during the pre-detonation phase) vs time for the three simulations. This plot demonstrates the expansion and contraction of the WD prior to detonation. The vertical lines mark the time at which a detonation occurred in each simulation. The sharp rise in density after the detonation is due to density enhancements by the detonation wave.

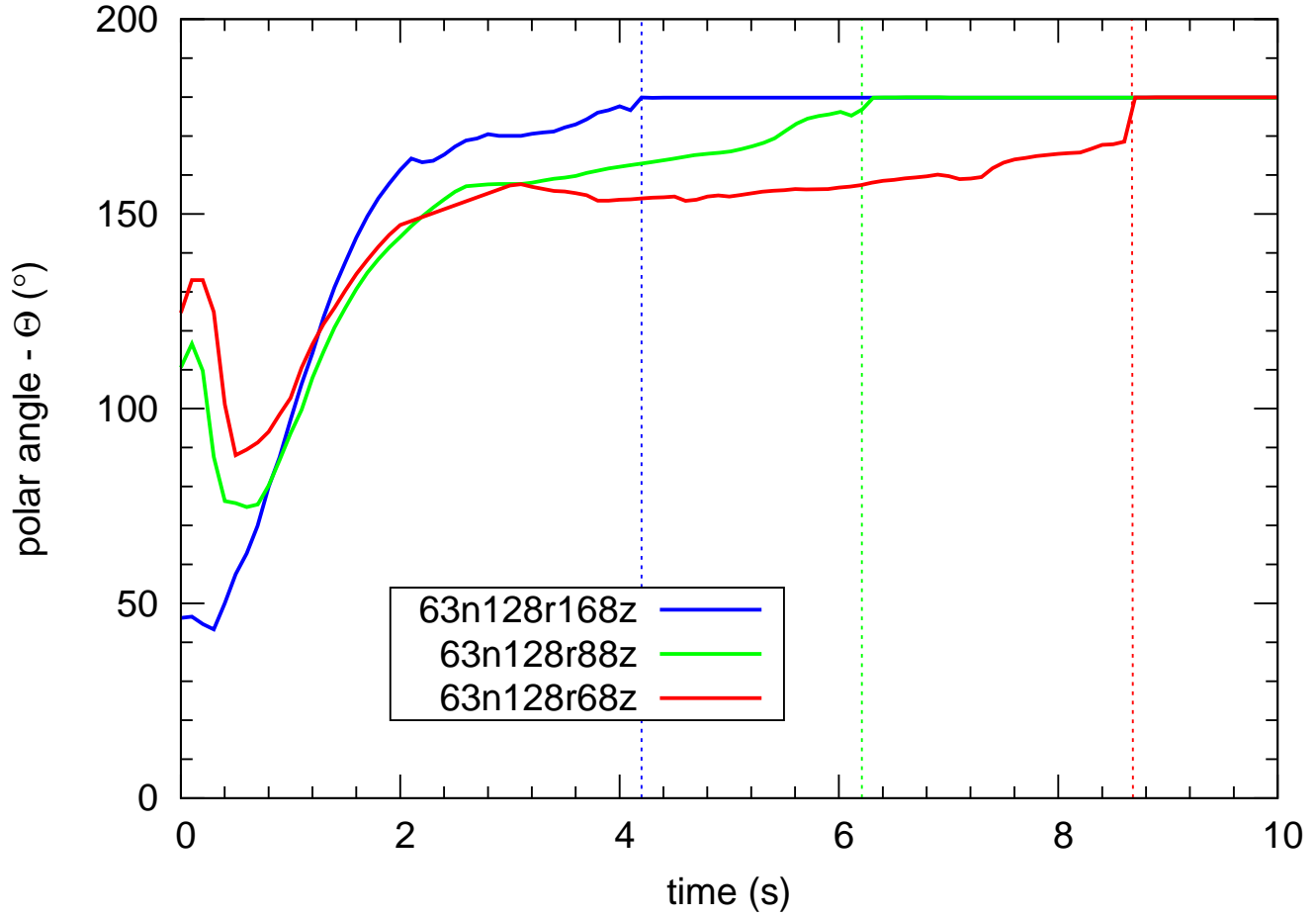


FIG. 5.— The polar angle, θ , of the leading edge of the ash vs time. This plot shows the progress of the fuel-ash mixture as it flows around the WD. Note that the initially large polar angles during the first second of evolution is due to the flame burning into the lower hemisphere of the WD. The vertical lines mark the time at which a detonation occurred in each simulation.

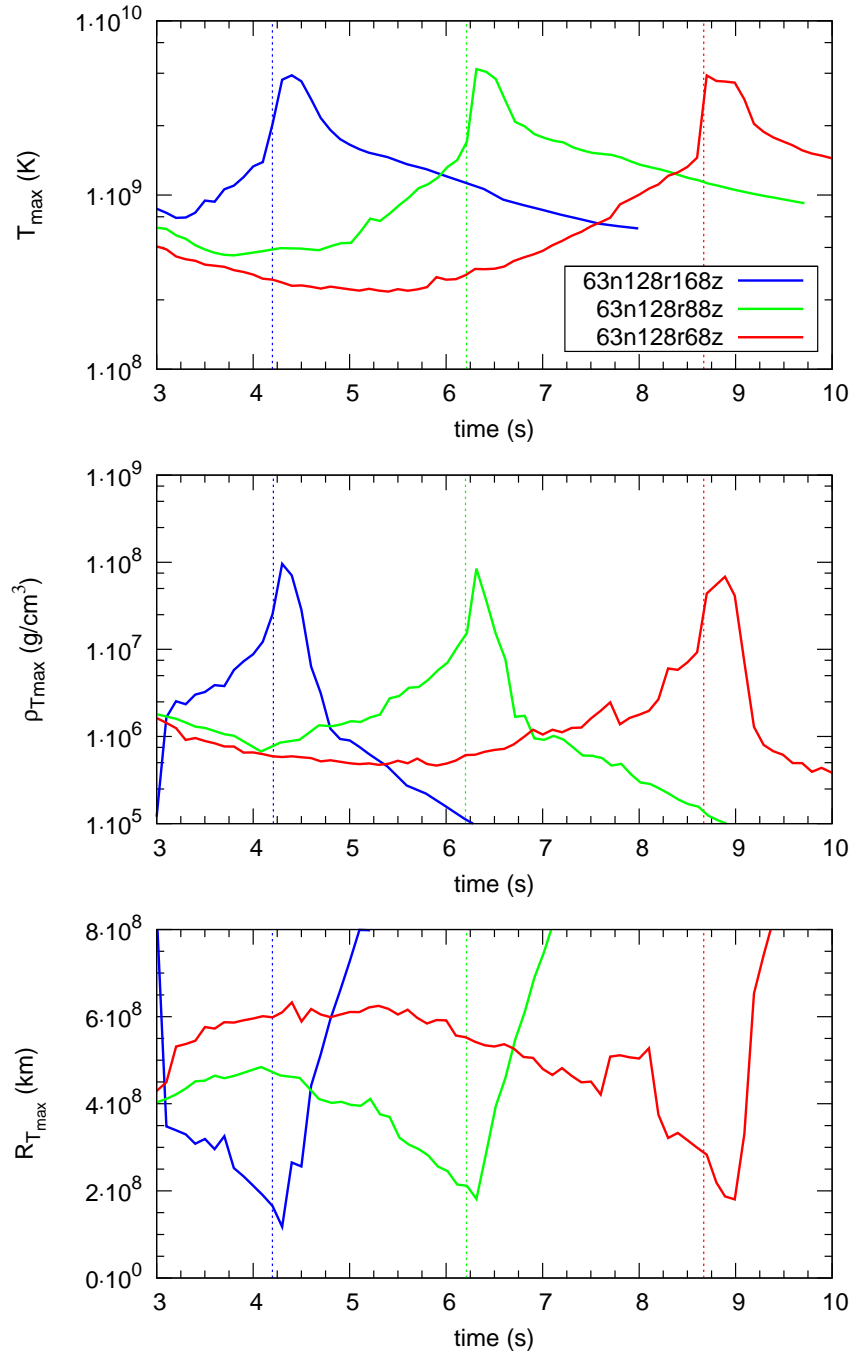


FIG. 6.— Conditions in the collision region: (*top*) The temperature of the computational cell with the maximum temperature in the collision region and whose material was composed of the fuel-ash mixture. The maximum temperature is plotted as a function of time. (*middle*) The density of the computational cell selected with the criteria described in the top figure as a function of time. (*bottom*) The radius of the computational cell selected with the criteria described in the top figure as a function of time. The vertical lines mark the time at which a detonation occurred in each simulation.

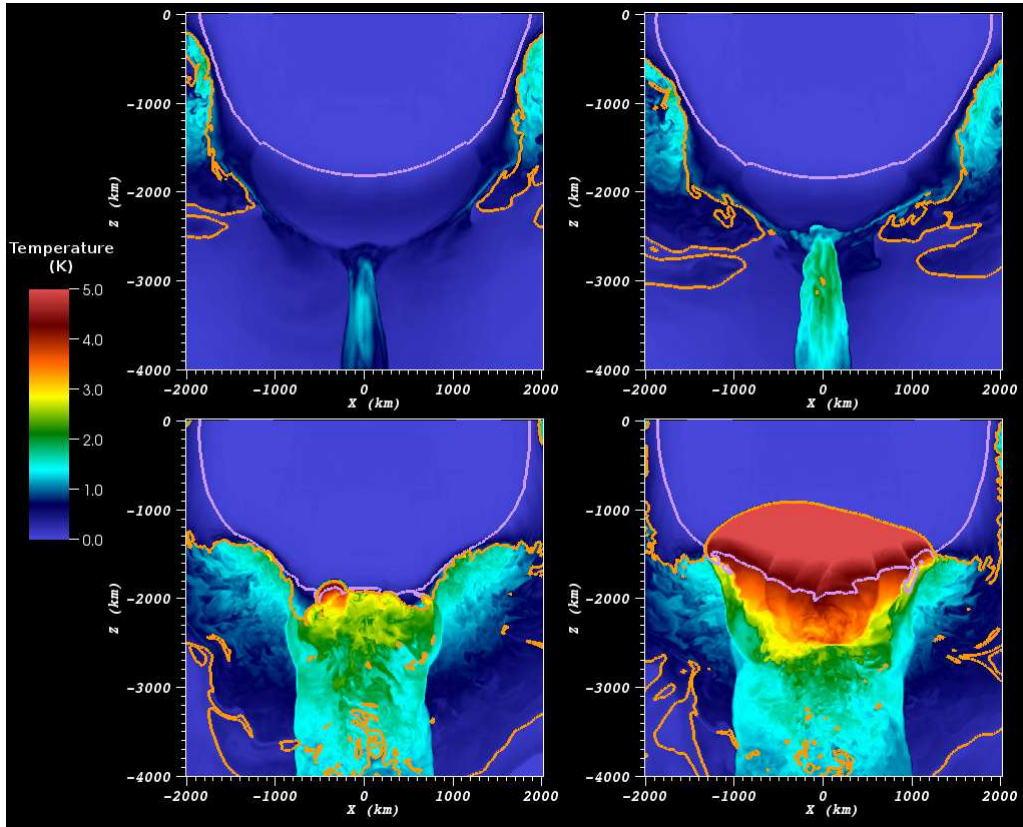


FIG. 7.— Slice images of the lead up to detonation of the classical GCD model of SNe Ia. This model is the *16b100o8r* detailed in J08. The four images are of the bottom hemisphere of the white dwarf. The slice plane is the x - z plane. The magenta contour is a density contour at $\rho = 1.0 \cdot 10^7 \text{ g/cm}^3$ - the nominal density at which hot C/O would detonate. The orange contour delineates material that is pure fuel from material that contains ash (e.g. ash that was converging on the collision region). The colors indicate temperature whose values correspond to the color bar on the left. The color bar is in units of 10^9 K . (*top left*) $t=1.8\text{s}$. Ash approaches the collision region and a hot region forms. (*top right*) $t=1.9\text{s}$. The ash converges further into the collision region. The hot region increases in temperature and begins to smolder. (*bottom left*) $t=2.22\text{s}$. The smoldering fuel has pushed into the region with $\rho > 1.0 \times 10^7 \text{ g/cm}^3$ and a detonation has just formed. (*bottom right*) $t=2.3\text{s}$. The detonation has spread from where it initially started. The high temperature region as well as the smooth detonation front is visible.

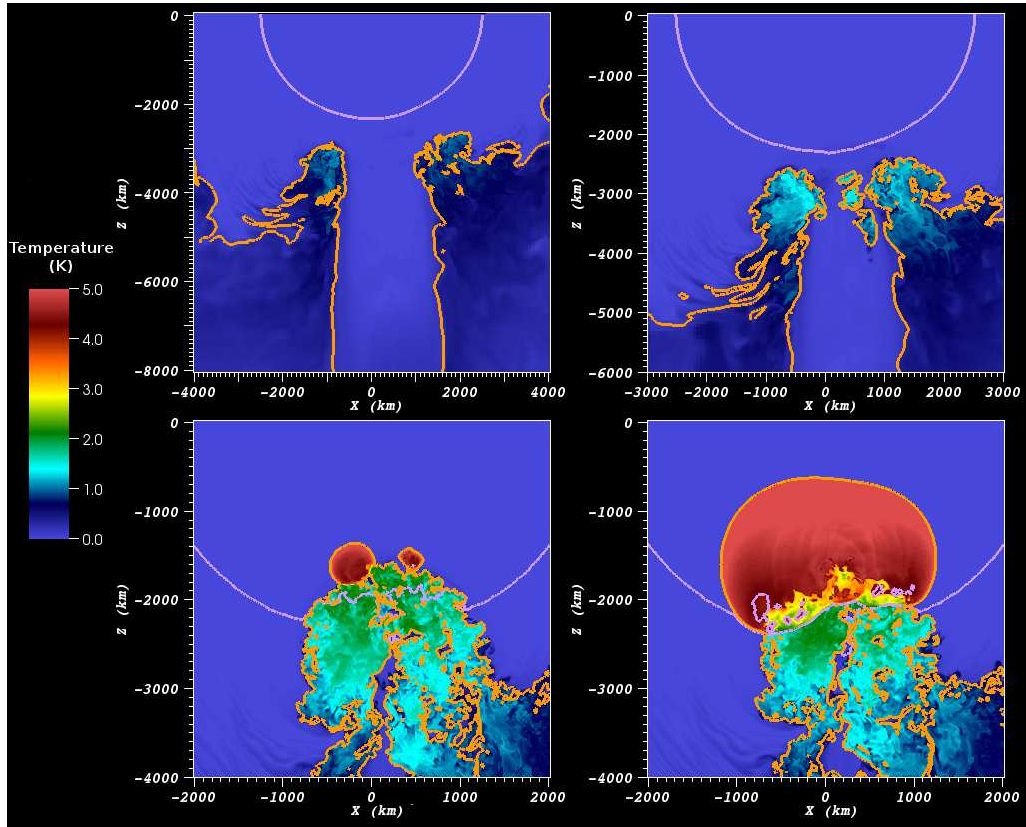


FIG. 8.— Slice images of the lead up to detonation of the PGCD model of SNe Ia. This model is the $63n128r168z$. The four images are of the bottom hemisphere of the white dwarf. The slice plane is the x - z plane. The magenta contour is a density contour at $\rho = 1.0 \cdot 10^7$ g/cm^3 - the nominal density at which hot C/O would detonate. The orange contour delineates material that is pure fuel from material that contains ash (e.g. ash that was converging on the collision region). The colors indicate temperature whose values correspond to the color bar on the left. The color bar is in units of 10^9 K. (*top left*) $t=3.5\text{s}$. Ash approaches the collision region. (*top right*) $t=3.8\text{s}$. Note that the figure is zoomed in from previous panel. The fuel-ash mixture continued to push into the collision region. The mixture heats since the WD was contracting and the ash was pushing to higher densities (*bottom left*) $t=4.23\text{s}$. Note that the figure is zoomed in from the previous panel. The mixture has reached the critical temperature and density and a detonation has just formed at several locations in the mixture. (*bottom right*) $t=4.3\text{s}$. The detonation wave is spreading through the star. The high temperature region behind the detonation wave as well as the smooth detonation front are clearly visible.

TABLE 1
LIST OF SIMULATIONS AND THEIR PROPERTIES

sim name	Δx^a (km)	n_{ign}^b	r_{ign}^c (km)	z_{ign}^d (km)	$E_{nuc,def}^e$ (10^{49} ergs)	$E_{nuc,def}^f$ ($E_{binding}$)	$\rho_{c,min}^g$ (10^7 g/cm 3)	$t_{\rho_{c,min}}^h$ (s)	t_{det}^i (s)	R_{det}^j (km)	$E_{kinetic}^k$ (10^{51} ergs)
63n128r168z	8	63	128.0	168.0	18.9	0.38	3.51	3.10	4.20	1,630	1.23
63n128r88z	8	63	128.0	88.0	29.1	0.59	1.13	3.83	6.21	2,124	1.19
63n128r68z	8	63	128.0	68.0	38.6	0.78	0.43	4.71	8.67	2,660	1.05

^a Maximum spatial resolution of the simulation.

^b Number of ignition points.

^c Radius of the spherical volume containing the ignition points.

^d Location along the z-axis of the origin of the spherical volume containing the ignition points.

^e Amount of energy released during the deflagration phase.

^f Amount of energy released during the deflagration phase as a fraction of the binding energy of the WD.

^g Central density of the WD at maximum expansion.

^h Time at which the WD reaches maximum expansion.

ⁱ Time at which the WD detonates.

^j Radius of the location where the detonation is initiated in the WD.

^k Kinetic energy contained in post-explosion nebula.

TABLE 2
FINAL YIELDS FROM SIMULATIONS WITH MULTIPLE IGNITION POINTS.

sim name	$X(^{12}\text{C})$ M_{\odot}	$X(^{16}\text{O})$ M_{\odot}	$X(^{24}\text{Mg})$ M_{\odot}	$X(\text{Si-group})$ M_{\odot}	$X(\text{NSE})$ M_{\odot}
<i>63n128r168z</i>	0.064	0.099	0.030	0.19	0.98
<i>63n128r88z</i>	0.091	0.14	0.045	0.20	0.89
<i>63n128r68z</i>	0.13	0.19	0.062	0.27	0.72

TABLE 3
DEFLAGRATION PRODUCTS OF SIMULATIONS WITH
MULTIPLE IGNITION POINTS.

sim name	$X(^{24}\text{Mg})$ M_{\odot}	$X(\text{Si-group})$ M_{\odot}	$X(\text{NSE})$ M_{\odot}
<i>63n128r168z</i>	0.017	0.025	0.086
<i>63n128r88z</i>	0.022	0.033	0.142
<i>63n128r68z</i>	0.030	0.044	0.190